In Silico Analysis of Haemodynamics in Patient-Specific Left Atria with Different Appendage Morphologies

Andy L. Olivares[1], Etelvino Silva[2], Marta Nuñez-Garcia[1], Constantine Butakoff[1], Damián Sánchez-Quintana[3], Xavier Freixa[4], Jérôme Noailly[1], Tom de Potter[2], and Oscar Camara[1(✉)]

[1] Department of Information and Communication Technologies, Universitat Pompeu Fabra, Barcelona, Spain
oscar.camara@upf.edu
[2] Arrhythmia Unit, Department of Cardiology, Cardiovascular Center, Aalst, Belgium
[3] Department of Anatomy, University of Extremadura, Badajoz, Spain
[4] Department of Cardiology, Hospital Clinic de Barcelona, Universitat de Barcelona, Barcelona, Spain

Abstract. The influence of the left atrial appendage (LAA) and its different possible morphologies in atrial haemodynamics and thrombus formation is not fully known yet. The main goal of this work is to analyse blood flow characteristics in relation with LA/LAA morphologies to better understand conditions that may lead to thrombus formation. We constructed several patient-specific computational meshes of left atrial geometries from medical imaging data. Subsequently, Computational Fluid Dynamics (CFD) methods were run with boundary conditions based on pressure and velocity measurements from literature. Relevant indices characterizing the simulated flows such as local maps of vorticity were related to simple LAA shape parameters. Our in silico study provided different 3D haemodynamics patterns dependent on the patient-specific atrial geometry. It also suggests that areas near the LAA ostium and with presence of lobes are more prone to coagulation due to the presence of low velocities and vortices.

Keywords: Left atrial appendage · Shape analysis · Haemodynamics · CFD · Vorticity · Thrombus formation

1 Introduction

Atrial fibrillation (AF) is the most common sustained heart rhythm disorder and is one of the main causes of cerebral strokes [1]. In patients with non-valvular atrial fibrillation (NVAF), around of 90% of thrombi leading to stroke are originated in the left atrial appendage [2], which is an interesting anatomical structure with large inter-subject morphological variability. Percutaneous left atrial appendage (LAA) closure is a promising approach for stroke prevention, which is recommended for patients with contraindications to anticoagulant therapy. Due to the large inter-subject variability in LAA, an accurate morphological analysis of its geometry is crucial in selecting the appropriate device size during preoperative planning.

M. Pop and G.A. Wright (Eds.): FIMH 2017, LNCS 10263, pp. 412–420, 2017.
DOI: 10.1007/978-3-319-59448-4_39

The left atrial appendage acts as a decompression chamber during left ventricular systole and in periods of high left atrial pressure [3], but its functioning and the influence its morphology are still unclear. Studies relating blood flow dynamics with LA configurations (e.g. number, location, size and orientation of pulmonary veins, volume) and LAA morphologies (e.g. chicken wing, cactus, cauliflower, windsock [4]) may shed some light on the relevance of this structure, his role in the cardiovascular system and the long-term effect of its occlusion.

Advanced imaging techniques such as Computational Tomography (CT) or 3D Rotational Angiography (3DRA) provide accurate 3D reconstructions of LAA geometries. Blood flow information is usually measured from Transesophageal Echocardiographic (TEE) images (including Doppler acquisitions) after LAA occlusion interventions to evaluate if the device is correctly positioned, but they only provide partial flow data on a plane or a given point of view. A more complete haemodynamics characterization is possible using novel 4D-flow Magnetic Resonance Imaging (MRI) [5, 6], but it is still in its infancy. On the other hand, Computational Fluid Dynamics (CFD) techniques can create 3D blood flow simulations to study haemodynamics patterns in different LA/LAA configurations. A few number of papers [7–10] can be found in the literature with CFD studies on LA. They are basically performed on synthetic geometries or in 1-2 patient-specific geometries from CT/MR imaging, but without jointly analysing haemodynamics and morphological indices to investigate the risk of thrombus formation.

The main objective of this study was evaluating haemodynamics parameters in different patient-specific LA/LAA morphologies to identify characteristics potentially related to high risk of thrombus formation. Four geometrical models of the LA, each one with a different type of LAA morphology, were built from patient-specific 3DRA data. Simple morphological parameters parameterizing the LAA geometry (e.g. size, ostium diameters, number of lobes, volumes, lengths) were jointly analysed with indices characterizing blood flow patterns obtained from CFD simulations (e.g. velocities, vorticity, streamlines, Reynolds number, oscillating shear index, relative residence time), providing a complete overview of each LA/LAA configuration.

2 Materials and Methods

2.1 Image Processing and Meshing

The computational pipeline for generating the set of CFD simulations started with the segmentation of patient-specific 3DRA images to obtain LA/LAA geometries. Left atrial meshes were obtained from imaging data of four AF patients (OLV Hospital, Aalst, Belgium). The ethical committee approved this study and informed consent was obtained from every patient. 3D Rotational Angiography images were acquired with an Innova 3D system (GE Healthcare, Chalfont St Giles, UK) and reconstructed with the scanner workstation, providing isotropic 3D images with 0.23 mm or 0.45 mm volumetric pixel size, for 512 or 256 pixels per dimension, respectively. Segmentation of the left atria was achieved with semi-automatic thresholding and region-growing algorithms available at the scanner console. From the resulting binary masks, surface meshes (with triangular elements) of the LAA were built with the classical Marching Cubes

method. A Taubin filter [11] was applied to smooth the surface mesh while preserving the original volume. The catheter, always present in the reconstructed mesh (see Fig. 1), was manually removed using MeshLab[1]. Subsequently, inlet and outlet surfaces were added using MeshMixer[2]: four synthetic pulmonary veins (i.e. tubes) were added as inlets whereas the mitral valve area was defined as outlet. Location and physical dimensions of these surfaces were determined following measurements from the 3DRA images. From the triangulated surface, the tetrahedral mesh was created with Gmsh[3]. Figure 1 illustrates some intermediate results during the left atrial meshing pipeline.

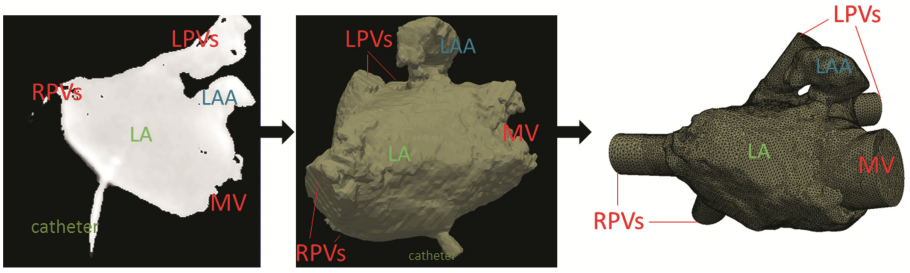

Fig. 1. Generation of left atrial meshes. Left: Segmentation of the left atria from 3DRA images. Middle: surface mesh after applying Marching cubes. Right: surface mesh after re-meshing, smoothing and adding appropriate inlet (PVs) and outlet (MV) surfaces. L: left; R: right; MV: mitral valve; PV: pulmonary vein. LAA: left atrial appendage.

2.2 Left Atrial Blood Flow Simulations

A second order implicit unsteady formulation was used for the solution of the momentum equations in the CFD simulations, in conjunction with a standard partial discretization for the pressure (under-relaxation factors of 0.3 and 0.7 for the pressure and momentum, respectively). Blood flow in the LA was modelled with the incompressible Navier–Stokes and continuity equations. Residuals of mass and momentum conservation equations lower than 0.001 were considered as absolute convergence criteria. Blood was modelled as an incompressible Newtonian fluid with density $\rho = 1060$ kg/m^3 [12]. The dynamic viscosity of blood in large vessels and the heart at normal physiological conditions was set to $\mu = 0.0035$ Pa-s [12]. Simulations were run using a laminar flow hypothesis under isothermal and non-gravitational effects. All walls were simulated rigid and with no-slip conditions, replicating the worst AF scenario (e.g. chronic AF), when atrial contraction is not possible anymore. The differential equations were solved using a time-step $\Delta t = 0.01$ s. At the inlets of the LA model (i.e. the four PVs) a time-varying blood flow function was applied (see Fig. 2a), following clinical observations from Fernandez-Perez et al. [13]. At the outlet (i.e. the mitral valve) a pressure of 8 mmHg [14] was imposed during the ventricular diastolic phase. In ventricular systole, the MV

[1] http://www.meshlab.net.
[2] http://www.meshmixer.com.
[3] http://gmsh.info/.

is closed; this was simulated as a wall boundary. The systolic and diastolic phase lasted 0.4 s and 0.65 s, respectively [13].

2.3 Geometrical Characterization of LA and LAA

Several indices were studied to characterise LAA shape (see Fig. 2b, c). They were inspired on measurements used by clinicians to determine the optimal LAA occluder dimensions and intervention planning: the maximum diameters (d1, d2), area and height of the ostium (equivalent to the landing zone concept); LAA depth was estimated as the length of a straight line (H0) from the middle of the LAA height (H) to the LAA apex (furthest point); and an index estimating the length of the LAA, $\tau = H/2 + H0$ (higher values of τ indicate longer blood flow pathways, from the ostium to the apex of the LAA).

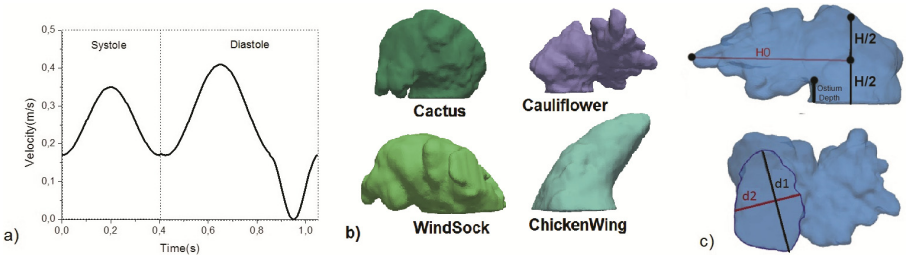

Fig. 2. (a) Generic blood velocity waveform applied to the pulmonary veins during ventricular systolic and diastolic phases. (b) the four typical LAA morphologies studied. (c) geometrical parameters of LAA, including its length and depth (H0 + H/2 and H, respectively) as well as ostium maximum diameters (d1 and d2).

2.4 Haemodynamics Indices Related to Thromboembolic Risk

The local Reynolds number was estimated from CFD simulations to determine the flow regime of blood towards the left ventricle. Mean flows and pressure waves were retrieved for a whole cardiac cycle at the inlets and outlets of the LA (e.g. PVs and MV) as well as in the LAA. LAA velocities < 0.55 m/s have been associated with a higher risk of stroke, with decreasing velocities of < 0.20 m/s being linked to the identification of thrombus within the LAA and a higher incidence of thromboembolic events [15]. Velocity streamlines of simulated flows were used to visually analyse the fluid dynamics profiles coming from left or right PVs. Vorticity maps, estimated from the second variant of the velocity gradient tensor (Q-criterion), were also computed to identify regions with high risk of thrombus formation. Thresholds on the Q-criterion (200-300 s^{-2}) were applied for vortex visualization purposes, similar to Otani et al. [10], to identify vortices associated to blood rouleaux or coagulation [3]. Paraview[4] was used for visualization and post-processing of CFD simulations.

[4] http://www.paraview.org.

3 Results and Discussion

Table 1 summarises the main geometrical and haemodynamics parameters characterising the four studied LA/LAA morphologies. LAA morphologies were classified into the usual four categories following the criteria of De Biase et al. [4]: case 1, cactus (CACT); case 2, cauliflower (CF); case 3, windsock (WS); and case 4, chicken wing (CW). Table 1 shows the variability of the studied morphologies, including large differences in LA volumes (from 131 to 220 cm^3), PV areas (from 14.9 to 29.1 cm^2), LAA ostium areas (estimated from diameters d1 and d2, from 3.13 to 6.15 cm^2), LAA volumes (from 7.7 to 14.8 cm^3), LAA landing zones (H from 1.27 to 2.35 cm), LAA lengths (from 3.35 to 4.45 cm) and number of lobes (from none to seven), among others. These measurements corresponded to the end diastolic phase, when the contrast in 3DRA acquisitions was filling the atria.

A simple verification of the obtained CFD simulations was achieved by comparing the peak of transmitral velocities in diastole (see Fig. 3a) with the ones provided by Fernandez-Perez [13], since we used the same inlet (PV) boundary conditions. Even though LA morphologies were quite different in both studies, transmitral velocities were

Table 1. LA/LAA geometrical and haemodynamics parameters. Volumes (V), areas (A), left and right pulmonary veins (LPV and RPV), mitral valve (MV), ostiumarea and depth (OsA and OsD), LAA depth and length (H, H0, τ), number of lobes (Nlobes), time-average wall shear stress (TAWSS), oscillating shear index (OSI), relative residence time (RRT), Reynolds number (Re). Bold values indicate the maximum/minimum (red/blue colours) among the 4 cases.

Geometrical Parameters	1	2	3	4	Haemodynamic Parameters	1	2	3	4
V_{LA} (cm^3)	**131**	147	**220**	157	E/A ratio (-)	**2.05**	**2.43**	2.34	2.33
V_{LAA} (cm^3)	13.9	8.7	**7.7**	**14.8**	Mean Blood flow Volume at the MV (cm^3)	**72.3**	101.0	**108.0**	85.8
LPV (cm^2)	1.53	2.08	**2.52**	**1.49**	$TAWSS_{LA}$ (Pa)	0.55	0.45	**0.72**	**0.26**
RPV (cm^2)	2.36	2.13	**2.91**	**2.06**	OSI_{LA} (-)	0.35	0.31	**0.27**	**0.36**
MV (cm^2)	**6.04**	7.05	7.97	**8.16**	RRT_{LA} (Pa^{-1})	5.9	5.7	**3.1**	**14.0**
OsA (cm^2)	3.77	**3.13**	4.96	**6.15**	$TAWSS_{LAA}$ (Pa)	**0.12**	0.06	0.05	**0.03**
H (cm)	**2.35**	1.80	**1.27**	1.95	OSI_{LAA} (-)	**0.35**	0.33	0.31	**0.23**
H0 (cm)	**2.71**	3.16	2.72	**3.58**	RRT_{LAA} (Pa^{-1})	**26**	51	53	**56**
τ (cm)	3.88	4.06	**3.35**	**4.55**	Re peak (-)	225	234	**342**	**155**
OsD (cm)	0.55	0.48	**0.25**	**0.80**	Case 1: Cactus (CACT); Case 2: Cauliflower (CF);				
Nlobes	3	**7**	3	**0**	Case 3: Windsock (WS); Case 4: Chicken Wing (CW).				

in the same range: 0.27–0.48 m/s and 0.33 m/s in our cases and Fernandez-Perez [13], respectively.

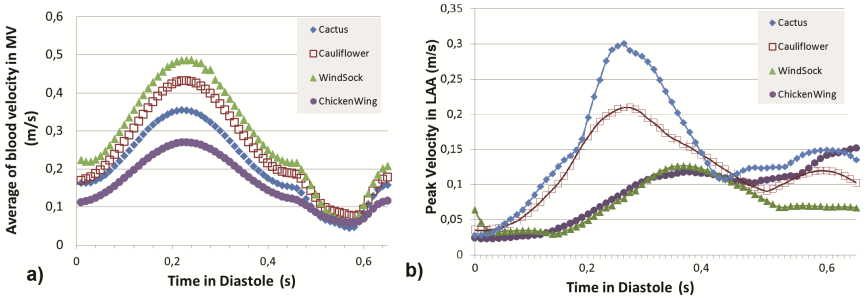

Fig. 3. Distribution of average blood velocity in the mitral valve (a) and the LAA ostium (b) during diastole.

The E/A ratio is a marker of diastolic performance of the heart, which is computed from the relation between early (E) to late (A) ventricular filling velocities. As expected, all E/A ratios estimated from CFD simulations are larger than two (E>>A), implying a restrictive and irreversible pattern in the LA [13]; in our case this is due to serious changes in LA elasticity and relaxation caused by AF. We also analysed peak diastolic (emptying) blood velocities in the LAA ostium (see Fig. 3b) since low values (<0.20 m/s) have been associated with the identification of thrombus [15]. In our experiments, case 1 (CACT, 0.30 m/s) and case 2 (CF, 0.21 m/s) presented a lower risk of thromboembolic events than case 3 (WS, 0.13 m/s) and case 4 (CW, 0.12 m/s), following the before mentioned criteria.

Figure 4 shows CFD-derived flow streamlines in two cases (case 1 and case 4, with cactus and chicken wing morphologies, respectively). It can be observed that blood flow enters the LAA mainly during systole, when the MV is closed. This shows the decompression role of the LAA in this cardiac phase, where higher pressures are found in the left atria. On the other hand, blood flow scarcely enters the LAA at the diastolic phase. Moreover, the LAA is preferentially filled in from flow coming from the LPV, while the RPV flow is mainly directed to the MV, in agreement with simulations from Vedula et al. [8].

Figure 5 displays the CFD-based vorticity maps of the four LA/LAA cases. Maps were thresholded within the range of 200–300 s^{-2} in the Q-criterion for visualization purposes, similarly to Otani et al. [10] (200 s^{-2} and 800 s^{-2} in their two cases); these maps are coloured with the magnitude of the blood flow velocities. Vortices were only created in the LAA during systole (closed MV) and highly depended on the underlying LA/LAA morphologies. Case 2, which had a Cauliflower LAA, was the one associated with more blood flow vortices and with a large number of secondary lobes. This is in agreement with the hypothesis relating the number of lobes with blood stasis and risk of thrombus formation. On the other hand, the Chicken Wing LAA (case 4) did not generated vortices, confirming clinical studies observing a lower risk of thrombosis in these morphologies. Furthermore, vortices with low blood flow velocities (dark blue in Fig. 5) were

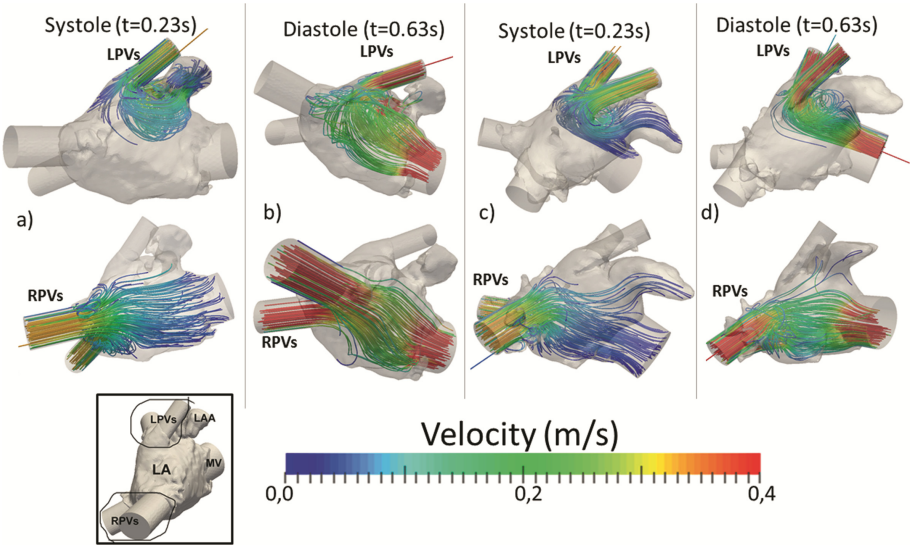

Fig. 4. Blood flow velocity streamlines with LPV (top) or RPV (bottom) origin at two time-points in systole and diastole. (a–b) Case 1 (cactus); (c–d) Case 4 (chicken wing).

consistently located around the LAA ostium or in small secondary lobes, potentially forming thrombus if blood flow is continuously slowed down in these areas.

The peak Reynolds (Re) numbers for the whole LA (see Table 1) remained in the blood laminar flow regime for the four cases, having a maximum and a minimum for the windsock (case 3) and chicken wing (case 4) morphologies, respectively. Case 3 had three secondary lobes and a very large LA (and PVs) compared with the other cases. This is probably caused by atrial remodelling due to AF, leading to an increased blood flow volume that may explain the largest Reynolds number. On the other hand, the chicken wing morphology (case 4) only had a single smooth main lobe, inducing low Re values.

Table 1 also summarises several indices related to CFD-derived wall shear stress such as the time-average wall shear stress (TAWSS), the oscillatory shear index (OSI) and the relative residence time (RRT), already used to assess the risk of thrombosis [9]. Case 4 (chicken wing) showed the lowest value for TAWSS in the LAA, which coincided with having only a main smooth lobe and the largest LAA volume. At the same time, this LAA morphology was associated with the largest RRT, implying the presence of areas where stagnation of blood flow is promoted. The largest value of the OSI index, associated to WSS vector deflection from blood flow predominant direction, was found in case 1; this was the cactus morphology, which had the most tortuous LAA, with its apex in the same plane than the ostium. Case 3 (windsock) also presented a relatively small TAWSS in the LAA even though it had the smallest LAA volume. One of the main characteristics of this case was its substantially larger LA and PV dimensions, leading to an increased blood flow volume (and higher TAWSS in the LA). This shows the relevance of analysing LAA haemodynamics considering the geometrical characteristics of the whole LA (and PV).

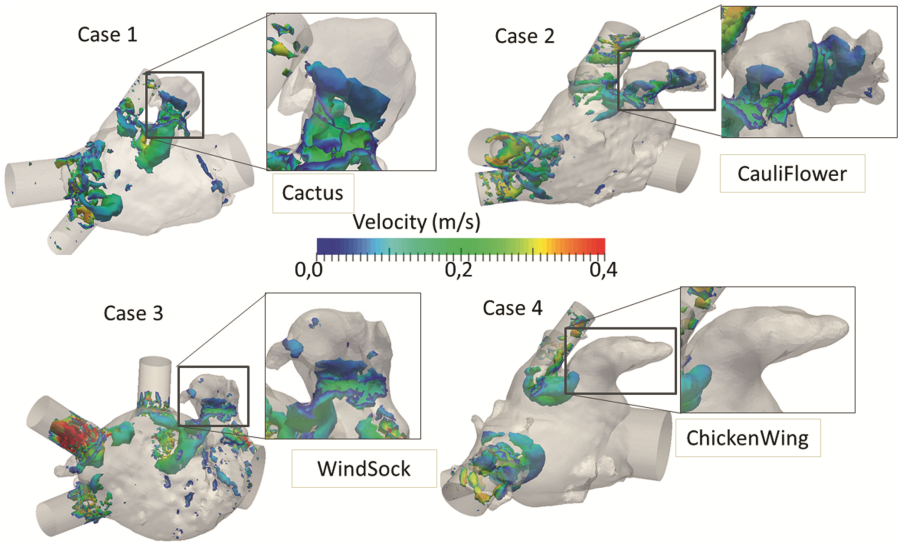

Fig. 5. Vorticity maps coloured by blood flow velocities in systole. Vortex values have been thresholded for visualization purposes (Q-criterion (200–300 s^{-2})). (Color figure online)

Case 3 will arguably be the hardest to implant a LAA occluder device due to the small landing zone area and an elevated presence of flow vortices.

4 Conclusions

Haemodynamics from CFD simulations and morphometric parameters from medical images were analysed in four patient-specific LA/LAA geometries corresponding to AF patients. A high number of secondary lobes and regions around the ostium were related with flow vortices and low velocities, which has been associated to high risk of thrombosis. Nevertheless, a deeper and more quantitative joint analysis of blood flow and geometrical indices is still required to better understand this process. Future work will focus on the validation of simulations with echocardiographic images and pressure measurements. Additionally, motion information will be included into the CFD simulations accounting for global and local mechanically derived changes (e.g. overall LA volume reduction and mitral valve ring displacement) in different phases of the cardiac cycle.

References

1. Wolf, P.A., Abbott, R.D., Kannel, W.B.: Original contributions atrial fibrillation as an independent risk factor for stroke: the framingham study. Stroke **22**, 983–988 (1991). doi: 10.1161/01.STR.22.8.983
2. Blackshear, J.L., Odell, J.A.: Appendage obliteration to reduce stroke in cardiac surgical patients with atrial fibrillation. Ann. Thorac. Surg. **61**, 755–759 (1996)

3. Al-Saady, N.M., Obel, O.A., Camm, A.J.: Left atrial appendage: structure, function, and role in thromboembolism. Heart **82**, 547–555 (1999)
4. Di Biase, L., Santangeli, P., Anselmino, M., et al.: Does the left atrial appendage morphology correlate with the risk of stroke in patients with atrial fibrillation? Results from a multicenter study. J. Am. Coll. Cardiol. (2012). doi:10.1016/j.jacc.2012.04.032
5. Markl, M., Lee, D.C., Furiasse, N., et al.: Atrial structure and function left atrial and left atrial appendage 4D blood flow dynamics in atrial fibrillation, 1–10 (2016). doi:10.1161/CIRCIMAGING.116.004984
6. Dyverfeldt, P., Bissell, M., Barker, A.J., et al.: 4D flow cardiovascular magnetic resonance consensus statement. J. Cardiovasc. Magn. Reson. **17**, 72 (2015). doi:10.1186/s12968-015-0174-5. Official journal of the Society for Cardiovascular Magnetic Resonance
7. Zhang, L.T., Gay, M.: Characterizing left atrial appendage functions in sinus rhythm and atrial fibrillation using computational models. J. Biomech. **41**, 2515–2523 (2008). doi:10.1016/j.jbiomech.2008.05.012
8. Vedula, V., George, R., Younes, L., Mittal, R.: Hemodynamics in the left atrium and its effect on ventricular flow patterns. J. Biomech. Eng. **137**, 1–8 (2015). doi:10.1115/1.4031487
9. Koizumi, R., Funamoto, K., Hayase, T., et al.: Numerical analysis of hemodynamic changes in the left atrium due to atrial fibrillation. J. Biomech. (2015). doi:10.1016/j.jbiomech.2014.12.025
10. Otani, T., Al-Issa, A., Pourmorteza, A., et al.: A computational framework for personalized blood flow analysis in the human left atrium. Ann. Biomed. Eng. **44**, 3284–3294 (2016). doi:10.1007/s10439-016-1590-x
11. Taubin, G.: Curve and surface smoothing without shrinkage. In: Proceedings of IEEE International Conference on Computer Vision, pp. 852–857 (1995). doi:10.1109/ICCV.1995.466848
12. Ku, D.N.: Blood flow in arteries. Annu. Rev. Fluid Mech. **29**, 399–434 (1997). doi:10.1146/annurev.fluid.29.1.399
13. Fernandez-Perez, G.C., Duarte, R., Corral de la Calle, M., et al.: Analysis of left ventricular diastolic function using magnetic resonance imaging. Radiologia **54**, 295–305 (2012). doi:10.1016/j.rx.2011.09.018
14. Nagueh, S.F., Appleton, C.P., Gillebert, T.C., et al.: Recommendations for the evaluation of left ventricular diastolic function by echocardiography. Eur. J. Echocardiogr. **22**, 165–193 (2009). doi:10.1093/ejechocard/jep007
15. Beigel, R., Wunderlich, N.C., Ho, S.Y., et al.: The left atrial appendage: anatomy, function, and noninvasive evaluation. JACC: Cardiovascular Imaging (2014). doi:10.1016/j.jcmg.2014.08.009